PERFORMANCE AND STABILITY OF DYE SOLAR CELLS ON STAINLESS STEEL

Doctoral Dissertation

Kati Miettunen

Helsinki University of Technology
Faculty of Information and Natural Sciences
Department of Applied Physics

TKK Dissertations 185
Espoo 2009

PERFORMANCE AND STABILITY OF DYE SOLAR CELLS ON STAINLESS STEEL
Doctoral Dissertation

Kati Miettunen

Dissertation for the degree of Doctor of Science in Technology to be presented with due permission of the Faculty of Information and Natural Sciences for public examination and debate in Auditorium K216 at Helsinki University of Technology (Espoo, Finland) on the 23rd of October, 2009, at 12 noon.

Helsinki University of Technology
Faculty of Information and Natural Sciences
Department of Applied Physics

Teknillinen korkeakoulu
Informaatio- ja luonnontieteiden tiedekunta
Teknillisen fysiikan laitos

Abstract

This study is on nanostructured dye solar cells which are easy to manufacture and use low cost materials. Dye solar cells have conventionally been deposited on conductive glass sheets. To reduce the costs and enable roll-to-roll mass production, the glass substrates should be replaced with flexible metal and plastic substrates. The change of the substrates has a profound effect on the cell, e.g. on electrochemical properties, optics, temperature treatments, and lifetime which all change when using alternative substrates.

In this work, the focus is on using stainless steel and ITO-PET substrates in dye solar cells. The electrochemical characteristics of the substrates were analyzed and the need for additional coatings to improve the performance or the stability was evaluated. The optimization of the other cell components in different metal-plastic cell configurations was also examined. An important part of the work was to decouple the effects of the different cell components on the cell performance. For this purpose, a method to study individual electrode performance based on electrochemical impedance measurements of a complete cell is presented.

Issues related to the up-scaling of the cell, namely current collection and spatial performance distribution, are also covered in this work. A novel, segmented cells configuration is presented to study the spatial performance distribution. It was discovered that there are large variations in the cell performance leading to significant efficiency losses. The spatial distribution was linked with the usual electrolyte filling technique which resulted in an uneven distribution of a common electrolyte component, 4-*tert*-butylpyridine.

Finally, the lifetime of the stainless steel based cells was examined. Interestingly, the cells with stainless steel photoelectrode substrates aged much faster than those with stainless steel counter electrode substrates. To examine the aging mechanisms, a segmented cell design was also developed specially for the degradation studies. With the segmented cells, it could be confirmed that the degradation of the stainless steel photoelectrode cells was not due to changes in the electrolyte. The aging of the stainless steel counter electrode cells was, on the contrary, linked with the corrosion of the stainless steel substrate by the electrolyte.

VÄITÖSKIRJAN TIIVISTELMÄ	TEKNILLINEN KORKEAKOULU PL 1000, 02015 TKK http://www.tkk.fi

Tekijä   Kati Miettunen

Väitöskirjan nimi
Ruostumattomalle teräkselle valmistettujen väriaineaurinkokennojen hyötysuhde ja stabiilisuus

Käsikirjoituksen päivämäärä 05.06.2009	Korjatun käsikirjoituksen päivämäärä 09.09.2009

Väitöstilaisuuden ajankohta   23.10.2009

☐ Monografia	☒ Yhdistelmäväitöskirja (yhteenveto + erillisartikkelit)

Tiivistelmä
Tämä tutkimus keskittyy nanorakenteisiin väriaineaurinkokennoihin, joiden tärkeimmät ominaisuudet ovat niiden edullisuus ja valmistusmenelmien yksinkertaisuus. Väriaineaurinkokenno on perinteisesti rakennettu johtavaksi pinnoitetuille lasisubstraateille. Korvattaessa lasisubstraatit taipuisilla metalli- ja muovisubstraateilla kustannuksia pienennetään ja mahdollistetaan rullalta rullalle – tyyppinen massatuotanto. Substraattien vaihtamisella on laajat vaikutukset kennoon; esimerkiksi kennon sähkökemialliset ominaisuudet, optiikka, lämpötilaprosessoinnin käyttö valmistuksessa, elinikä ja virrankeräimet ovat erilaiset vaihtoehtoisilla substraateilla.

Koska substraattien valinnalla on merkittävä vaikutus kennojen muiden osien valmistukseen, tässä tutkielmassa lähtökohdaksi on valittu nimenomaan substraatit. Tutkittavaksi metallisubstraatiksi on valittu ruostumaton teräs ja muovisubstraatiksi ITO-PET. Työssä karakterisoidaan substraattien sähkökemialliset ominaisuudet ja arvioidaan lisäpinnoitteiden tarvetta paremman toiminnan tai stabiiliuden saamiseksi. Työssä käydään läpi myös muiden kennokomponenttien optimointia erilaisissa metalli-muovikennokonfiguraatioissa. Tärkeänä osana tutkimusta on erottaa eri kennon osien vaikutus kennon toimintaan ja tätä tarkastelua varten työssä paneudutaan esim. yksittäisen elektrodin kvantitatiiviseen tarkasteluun kokonaisesta kennosta mitatun impedanssidatan perusteella.

Työssä tarkastellaan myös kennokoon kasvattamiseen liittyviä seikkoja, tarkemmin sanottuna virrankeräystä ja spatiaalisia ilmiöitä. Spatiaalisten toimintaerojen selvittämiseen työssä esitellään uusi segmentoitu kennorakenne. Tutkimuksissa havaittiin, että kennoissa on merkittäviä hyötysuhdevaihteluja, jotka aiheuttavat huomattavia häviöitä kennon toiminnalle. Kennon epätasainen toimivuus voitiin linkittää nykyisestä elektrolyytin täyttötavasta aiheutuvaan yleisen elektrolyytin lisäaineen, 4-*tert*-butylpyridiinin, epätasaiseen jakaumaan.

Lopuksi perehdytään ruostumattomalle teräkselle tehtyjen kennojen ikääntymiseen. Kennojen, joissa terästä käytettiin valoelektrodin substraattina, havaittiin ikääntyvän huomattavasti nopeammin kuin niiden, joissa teräs oli vastaelektrodilla. Ikääntymismekanismien tutkimiseksi työssä esitellään myös siihen suunniteltu segmentoitu kennorakenne. Tällä voitiin verifioida, ettei teräsvaloelektrodikennojen heikkeneminen johtunut muutoksista elektrolyytissä. Teräsvastaelektrodikennojen puolestaan havaittiin kärsivän korroosiosta elektrolyytissä.

Preface

Contents

List of Publications

This thesis consists of an overview and of the following publications which are referred to in the text by their Roman numerals.

I   K. Miettunen, J. Halme, M. Toivola, and P. Lund, *'Initial Performance of Dye Solar Cells on Stainless Steel Substrates'* Journal of Physical Chemistry C 112 (2008) pp. 4011-4017.

II   K. Miettunen, J. Halme, P. Vahermaa, T. Saukkonen, M. Toivola, and P. Lund, *'Dye Solar Cells on ITO-PET Substrate with TiO$_2$ Recombination Blocking Layers'*, Journal of the Electrochemical Society 156 (2009) pp. B876-B883.

III   K. Miettunen, J. Halme, and P. Lund, *'Spatial distribution and decrease of dye solar cell performance induced by electrolyte filling'*, Electrochemistry Communications 11 (2009) pp. 25–27.

IV   K. Miettunen, J. Halme, and P. Lund, *'Segmented Cell Design for Improved Factoring of Aging Effects in Dye Solar Cells'*, Journal of Physical Chemistry C 113 (2009) pp. 10297-10302.

V   K. Miettunen, J. Halme, T. Saukkonen, T. Peltola, M. Toivola, and P. Lund, *'Performance Degradation of Dye Solar Cells on Flexible Stainless Steel Substrates'*, Accepted for publication in Proceedings of 24th European Photovoltaic Solar Energy Conference, 21-25 September, 2009, Hamburg, Germany.

VI   K. Miettunen, M. Toivola, J. Halme, J. Armentia, P. Vahermaa, and P. Lund, *'Optimization of Dye-Sensitized Solar Cells on Stainless Steel'*, Proceedings of 22nd European Photovoltaic Solar Energy Conference, 3-7 September, 2007, Milan, Italy, pp. 512-515.

Related publications by the author not included in the thesis:

J. Halme, K. Miettunen, and P. Lund, *'Effect of Nonuniform Generation and Inefficient Collection of Electrons on the Dynamic Photocurrent and Photovoltage Response of Nanostructured Photoelectrodes.'*, Journal of Physical Chemistry C, 112 (2008) pp. 20491-20504.

M. Toivola, J. Halme, K. Miettunen, K. Aitola, and P. Lund, *'Nanostructured dye solar cells on flexible substrates – Review'*, International Journal of Energy Research, 33 (2009) pp. 1145-1160.

M. Toivola, T. Peltola, K. Miettunen, J. Halme, and P. Lund, *'Thin film nano solar cells - from device optimization to upscaling'*, Journal of Nanoscience and Nanotechnology, 10 (2010) pp. 1-7.

M. Toivola, K. Miettunen, J. Halme, F. Ahlskog, and P. Lund.*'Nanostructured Dye-Sensitized Solar Cells on Flexible Substrates Using Industrially Scalable Manufacturing Methods.'* Proceedings of 21st European Photovoltaic Solar Energy Conference, 4-8 September, 2006, Dresden, Germany, pp. 47-52.

H. Guangseng, J. Halme, K. Miettunen, M. Toivola, P. Lund, *'The performance enchancement by back reflection in nanostructured dye-sensitized solar cells'*, Proceedings of ISES World Congress 2007, 18-21 September, 2007, Beijing, China, pp. 1055-1058.

M. Toivola, K. Miettunen, J. Halme, and P. Lund. *'Thin Nanostructured Solar Cells on Metal Sheets'* Proceedings of 11th NSTI Nanotech Conference, 1-5 June, 2008, Boston, USA, pp. 96-99.

M. Toivola, T. Peltola, K. Miettunen, J. Halme, K. Aitola, and P. Lund, *'Large Area Optimized Thin Film Nano Solar Cells on Metal Sheet'*, Proceedings of 12th NSTI Nanotech Conference, 3-7 May, 2009, Houston, USA, pp. 126-129.

Author's contribution

The author was mainly responsible for all parts in Publications I-VI. Dr. Janne Halme contributed to the writing process, in particular to Publication I. The idea of using segmented cells for aging studies came from Dr. Janne Halme, and the segmented cells for Publications III and IV were designed together with him and the author. He also gave comments to research plans and analysis of the results. Mr. Tapio Saukkonen did the SEM, EDS, and EBSD measurements and analyzed their results with the author (Publications II, VI and V). Mrs. Paula Vahermaa contributed to the preparation of the experimental work for Publication II and VI. Ms. Toivola and Mr. Armentia conducted some experiments for Publication VI. Prof. Peter Lund (Publications I-VI), Ms. Minna Toivola (Publications I, II, V and VI), and Mrs. Paula Vahermaa (Publication II) commented the manuscripts to improve their quality.

List of Abbreviations

ALD	atomic layer deposition
AM1.5G	incident air mass 1.5 global spectrum
CE	counter electrode
CIGS	copper-indium-gallium selenide
CPE	constant phase element
D	dimension
DSC	dye solar cell
EBSD	electron backscattered diffraction
EDS	energy dispersive x-ray spectroscopy
EIS	electrochemical impedance spectroscopy
HOMO	highest occupied molecular orbital
I^-	iodide
I_3^-	tri-iodide
ITO	indium tin oxide
LUMO	lowest unoccupied molecular orbital
MPP	maximum power point
OC	open circuit
OCVD	open circuit voltage decay
PE	photoelectrode
PEDOT	poly(3,4-ethylenedioxythiophene)
PET	poly(ethylene terephalate)
PSS	poly(styrenesulfonate)
SEM	scanning electron microscopy
SRC	Standard Recording Conditions
StS	stainless steel
SU	substrate
TCO	transparent conducting oxide
TiO_2	titanium dioxide
TsO	*p*-toluenesulfonate
PV	photovoltaic
PVdF-HFP	poly(vinylidenefluoride-*co*-hexafluoropropylene)
XRD	x-ray diffraction

List of Symbols

c_{I3-}	concentration of I_3^- ions
d	thickness of the TiO_2 layer
D_{I3-}	diffusion coefficient of the I_3^- ions
CPE_{CE}	CPE which describes the double layer charging at the CE/electrolyte interface
CPE_{CO}	CPE which describes the double layer charging at the PE substrate/TiO_2 interface
CPE_{CT}	CPE which describes the double layer charging at the TiO_2 / electrolyte interface
CPE_{SU}	CPE which describes the double layer charging at the PE substrate/electrolyte interface
e	elementary charge
E_g	energy gap between HOMO and LUMO energy levels
F	Faraday constant
f	frequency
FF	fill factor
f_{min}	the frequency of the minimum value of the PE peak
j	imaginary unit
i	current density
i_{MPP}	current density at the maximum power point
i_{SC}	short-circuit current density
i_{lim}	limiting current density
k_B	Boltzmann coefficient
l	distance between the electrodes
n	number of electrons transferred in each reaction
P_{in}	power density of the incident illumination
R_{CE}	charge transfer resistance at the CE/electrolyte interface
R_{CO}	charge transfer resistance at the TiO_2/PE substrate interface
R_{CT}	charge transfer resistance at the TiO_2/electrolyte interface
R_s	series resistance
R_{SU}	charge transfer resistance at the PE substrate/electrolyte interface
R_t	electron transport resistance in the TiO_2 layer
T	temperature
t	time
V_{MPP}	voltage at the maximum power point
V_{OC}	open circuit voltage
Z_d	diffusion impedance of the electrolyte
Z_{CPE}	impedance of the constant phase element
Q	CPE_{CT} pre-factor
β	CPE_{CT} exponent
λ	wavelength
η	conversion efficiency
τ_{eff}	effective electron lifetime

1 Introduction

1.1 Why Photovoltaics?

One-fourth of the world's population does not have access to electricity [1]. In addition, both the world population and energy consumption are constantly growing. The growing needs of electricity cannot be fulfilled with fossil fuels in a sustainable way: Firstly, oil and natural gas reserves are limited. Secondly, coal resources are excessive, but their use produces large CO_2 emissions, the capture of which is still expensive. Thirdly, nuclear power is practically CO_2 free, but there are serious questions with the disposal of the nuclear waste, nuclear proliferation, and safe operation. To solve this situation, the share of renewable energy needs to be increased. Being a local energy source, renewable energy addresses most energy security and sustainability concerns.

Some of the renewable energy resources, such as hydroelectric power, wind power, and geothermal energy, are largely dependent on site conditions and their use is thus limited. Biofuels seem to be in a collision course with food supply; the use of land and water for biomass crop may severely conflict with cultivation of edible crops. Contrary to those, solar energy is spatially one of the most evenly distributed energy source and, conveniently, its potential is largest in the areas where the energy consumption is growing fastest. Photovoltaic conversion (PV) is perhaps the most elegant electricity production technology since PV modules do not contain any moving components. The absence of moving parts in PV modules results in advantages such as a very long lifetime and low maintenance requirements. The main remaining challenge with solar energy is the cost.

Learning curve forecasts show that the price reduction of PV could be faster compared to the other renewables [2]. In many energy scenarios, the proportion of solar energy is estimated to grow enormously in the coming decades. For instance, in the recent Shell Scenario [3], the share of solar energy of all primary energy is estimated to be 10 % in 2050. Efforts are, however, required to realize these predictions. Most of the present PV is based on single or multicrystalline silicon and in the preparation, large amounts of ultra-pure and expensive silicon is required. Thin film PV, such as copper-indium-gallium selenide (CIGS) or amorphous silicon, needs a much smaller amount of photoactive materials and they can be deposited on larger surfaces than the traditional silicon cells. However, to speed up the implementation of solar energy radically, cheaper PV technologies need to be developed and introduced to the market. Therefore the study of next generation PV, such as dye solar cells and polymer cells based on novel physical structures, is highly motivated. These next generation PV cells are prepared mainly from inexpensive materials and with some material combinations even roll-to-roll mass production is feasible.

13

1.2 Background and Scope of This Study

The aim of dye solar cells (DSC) is to provide a cheaper alternative to conventional solar cells; the manufacturing methods of DSCs are rather simple and the materials are cheap and their availability is good. DSCs have traditionally been deposited on glass substrates with a transparent conductive oxide (TCO) coating. These are in fact the most expensive DSC components [4]. In addition, the rigidness and fragility of the glass substrates cause restrictions to the production by requiring batch processing. To enable roll-to-toll mass production and to reduce the costs, the use of flexible substrates such as metals and polymers has been introduced. For instance, stainless steel has been estimated to be even 25 % cheaper than TCO glass [5].

The use of alternative substrates is interesting also from the applications point of view. Due to the large variety of cell colors available, DSCs have important advantages also in architectural applications and design products. Semi-transparent DSCs prepared on plastics could be used e.g. as transferable façade elements which could be fastened to a window. With such elements, the exterior and interior design could be easily altered. DSCs prepared on metal could serve, for instance, as a roofing material.

The selection of suitable metal substrates is severely limited by the stability: most metals, for instance copper, corrode in the iodine containing DSC electrolyte [6-8]. Stainless steel (StS) is the cheapest metal which has passed electrolyte soaking tests [6-8]. The conductivity of StS is superior compared to TCO as it is four orders of magnitude larger [6, 7], even though StS is not even a highly conducting metal.

Metal substrates were first employed as counter electrode (CE) substrates [6-8] since it is optically beneficial to use a transparent substrate, plastic in flexible cells, as a photoelectrode (PE) substrate. The plastic substrates, however, require low temperature processing and these methods have not been as successful as high temperature sintering in the PE preparation [9-10].

There are, however, several good low temperature techniques, such as chemical deposition [11] and sputtering, for the preparation of a high performance CE. Since metal substrates withstand high temperatures, placing metals on the PE and plastics on the CE has become a popular cell configuration [11-13]. In the metal PE setup, there are additional optical losses because the light has to also penetrate the CE and the bulk electrolyte.

The purpose of this study is to determine the performance and stability limiting factors in flexible DSCs. The focus is on the issues specific for the flexible DSCs, in particular stainless steel based DSCs. From the issues that concern the DSCs field in general, only those previously unknown are covered. In other words, the aim of this thesis is to find the most important questions related to the flexible DSCs.

In this contribution, the cell design starts from the substrates: stainless steel and indium tin oxide coated poly(ethylene terephalate) (ITO-PET) plastic. The substrate centered

approach is chosen because the substrates largely determine the preparation of the other cell components. The study begins with the examination of the charge transfer between the substrate and other cell components. From there, the study is expanded to the optimization of other cell components. Then, the up-scaling issues, such as spatial performance distribution and current collection, are covered. Finally, the lifetime of the stainless steel based DSCs is examined.

1.3   Outline of This Thesis

The thesis is divided into five chapters. In Chapter 1, the introduction, the motivation, and the background for this study are presented. The basics of dye solar cells are discussed in Chapter 2. In Chapter 3, the experimental methods are described and there the novel segmented cell configuration as well as electrochemical impedance spectroscopy measurements are discussed in detail. The results are presented in Chapter 4. In addition to the short review of the state of the art in Chapter 1, a more detailed literary review on each studied subject is given in the results section (Chapter 4). The conclusions are presented in Chapter 5. The thesis is based on the six original Publications listed on page 13.

2 Basics of Dye Solar Cells

2.1 Operating Principles of Dye Solar Cells

The schematics of the conventional DSCs are illustrated in Figure 2.1. In DSCs, the dye transfers the energy of photons to electrons. In the photoexcitation, an electron leaps from the highest occupied molecular orbital (HOMO) to the lowest unoccupied molecular orbital (LUMO) of the dye. The energy gap E_g between HOMO and LUMO energy levels defines the maximum absorption wavelength for photoexcitation. Only the amount E_g of the photon energy can be used and therefore the theoretical maximum voltage of the cell is E_g/e.

The dye molecules are attached to a nanoporous TiO_2 film which has a very large surface area. The excited electrons are injected to the TiO_2 conducting band. The electrons travel by diffusion through the nanocrystalline TiO_2 to the conducting surface of the substrate. The preceding materials form together the photoelectrode (PE) which is the anode of the cell. In practice, the maximum voltage of a DSC is determined by the redox potential of the electrolyte and the Fermi level of the TiO_2 film as indicated in Figure 2.1.
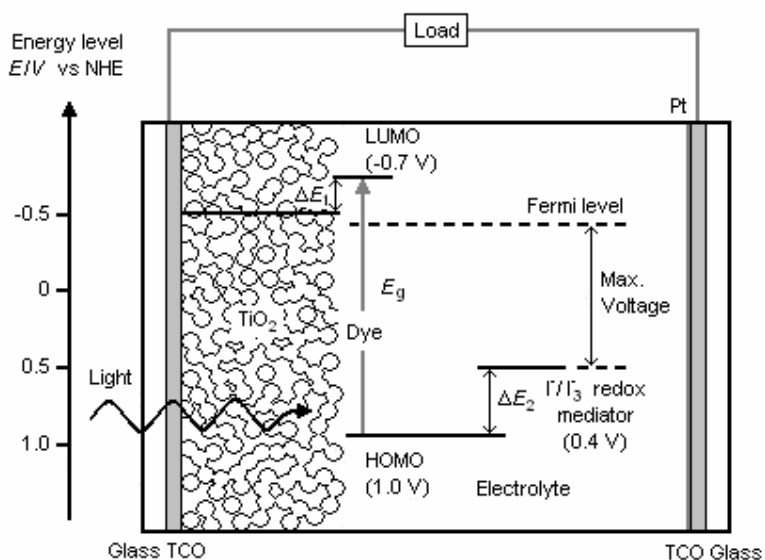
Figure 2.1   **The structure of a conventional DSC and the energy level scheme (not in scale). Modified from the one presented in literature [14].**

The conducting surface of the anode is connected through an external load to the cathode which is also called the counter electrode (CE). Typically, a CE consists of a conductive substrate coated with a catalyst layer, most commonly Pt. The catalyst accelerates the reaction in which tri-iodide (I_3^-) is reduced to iodide (I^-) ions:

$$I_3^- + 2e^- \rightarrow 3I^- \tag{1}$$

The I^- ions diffuse to the PE where the dye accepts electrons from them and oxidizes them back to I_3^- ions. In the ideal operation of a DSC, no permanent chemical transformations take place.

2.2 Photovoltaic Characteristics

The photovoltaic performance of a solar cell can be defined from a current density - voltage (*i-V*) curve. The *i-V* measurements are performed with a solar simulator typically in Standard Reporting Conditions (SRC) which refer to 1000 W/m^2 light intensity with AM1.5G spectra at 25 °C. The main photovoltaic performance characteristics of a solar cell are the open circuit voltage V_{OC}, the short-circuit current density i_{SC}, the fill factor *FF*, and the conversion efficiency η. V_{OC} is measured with zero current, and i_{SC} with zero voltage as shown in Figure 2.2. Note that in the Publications, the sign of V_{OC} changes according to the focus of the Publication; when the focus is on electrochemical characteristics, negative V_{OC} values are given, and when it is on cell performance in general, positive V_{OC} values are shown. The maximum power point (MPP) and the corresponding voltage V_{MPP} and current density i_{MPP} are also marked in Figure 2.2. *FF*, which describes the squareness of the *i-V* curve, is defined as

$$FF = \frac{V_{MPP} \cdot i_{MPP}}{V_{OC} \cdot i_{SC}} . \tag{2}$$

Knowing also the power of incident illumination to the active area of the cell P_{in}, η can be determined

$$\eta = \frac{V_{MPP} \cdot i_{MPP}}{P_{in}} = \frac{FF \cdot V_{OC} \cdot i_{SC}}{P_{in}} . \tag{3}$$
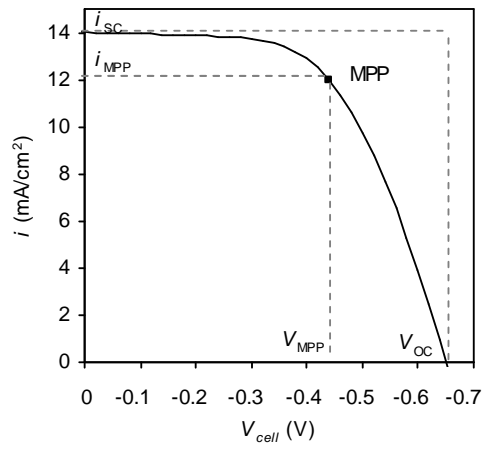
Figure 2.2   *i-V* **curve of a solar cell.**

3 Experimental Methods

In this work, the test samples were mainly different types of DSCs. In addition to complete solar cells, also other cell types were prepared to study a specific cell component. Substrate – counter electrode (SU-CE) cells were made to investigate the PE substrate performance, namely, recombination from the PE substrate. Counter electrode – counter electrode (CE-CE) cells were used in the study of the charge transfer at the CE and in the electrolyte. The structure schematics of the different cell types are illustrated in Figure 3.1. New segmented cell configurations were introduced to the study of spatial performance distribution and to the factoring of aging mechanisms. The segmented cells are discussed in Chapter 3.1. The details of the cell preparation are given in the Publications.

The measurement techniques in this work were mostly electrochemical: A standard technique is photovoltaic characterization with a solar simulator in SRC. Polarization also known as i-V measurements were conducted also in dark to determine e.g. the i-V curves of the SU-CE cells. Open circuit voltage decay (OCVD) [15] measurements were performed in Publications I-IV to study the electron lifetime at the PE. Electrochemical impedance spectroscopy (EIS) is a powerful tool for the separation of the electrochemical performance of different cell components and therefore it was used widely in the Publications. An important methodological aspect of this work is to show how quantitative comparison of the data of different cells can be made. Further discussion of the EIS measurements is presented in Chapter 3.2.

Some optical measurements were also made, mainly for the analysis of CEs described in Publication VI. Scanning electron microscopy (SEM) combined with element analysis, energy dispersive x-ray spectroscopy (EDS) (Publications IV-V), crystal structure analysis, and electron backscattered diffraction (EBSD) (Publication II) was also employed. X-ray diffraction (XRD) measurements were also made in Publication II. The specifics of the measurement equipment and the measurement parameters are given in the Publications.
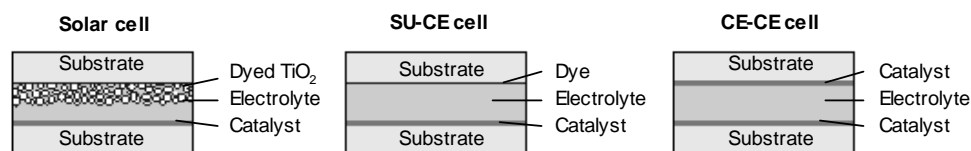
Figure 3.1   **The structure of a solar cell, a SU-CE cell, and a CE-CE cell.**

3.1   Segmented Cell Design

Segmented cells are divided to electrically isolated compartments sharing the same electrolyte. Some segmented structures have been used prior to this study, for instance, as an internal reference electrode [16]. In this contribution, new segmented cell designs were introduced for the examination of spatial performance distribution and aging.

3.1.1   Segmented cell for studying spatial performance distribution

Spatial performance distribution in DSCs has previously been studied with spatially resolved photocurrent imaging [17-19], which, according to its name, provides the distribution of i_{SC}. The most significant advantage of the segmented cell method is that it gives the spatial distribution of all the photovoltaic characteristics.

Here, 2-segment cells and 4-segment cells (Figure 3.2) were employed. The performance of the individual segments was compared to the performance of single cells with similar active area. Figure 3.2 shows a reference single cell for a 4-segment cell. The segments of the 2-segment cells were geometrically completely symmetric contrary to the segments of the 4-segment cells. In the 4-segment cells, there is asymmetry between the middle and the outer segments; for instance, the amount of electrolyte surrounding the active area is different. Hence, the 2-segment cells are better suited for quantitative analysis than the 4-segment cells. The 4-segment cells show, however, the trends in the spatial distribution in more detail since increasing the number of segments results in higher resolution. Further specifics of the segmented cell structure for the spatial distribution studies are given in Publication III.
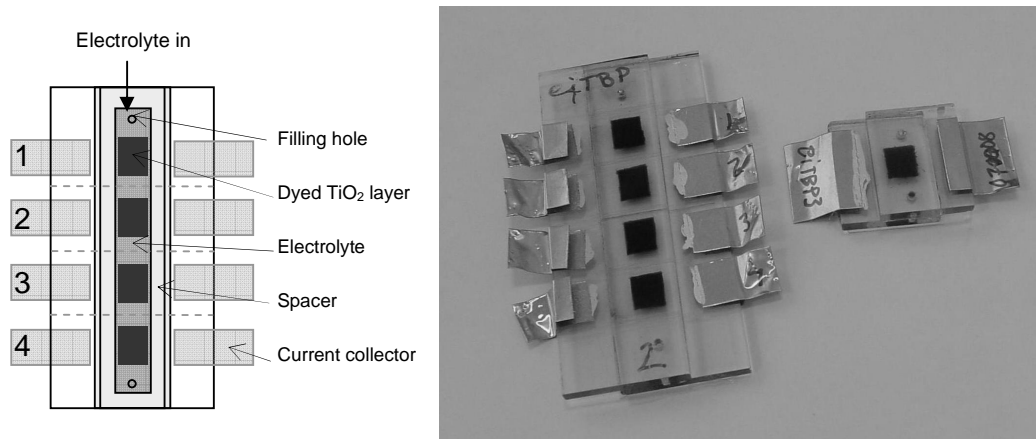
Figure 3.2   On the left schematics of a four segment cell and on the right a picture of a 4-segment cell and a single reference cell.

3.1.2 Segmented cell for aging studies

In aging studies the segmented cells can detect changes that are related to or transmitted by the electrolyte. This is because as the segments are sharing the electrolyte layer, changes in the electrolyte in one segment should cause changes in the other as well. An important benefit of using the segmented cells method compared to most of the spectroscopic analysis methods is that it does not require dismantling of the cell, which enables continuous examination of the degradation.

In Publication IV, the time constant for the segment cell, i.e. the period of time in which the segments should affect each other, is derived with both experiments and calculations. Both techniques indicated that the constant for the segmented cell design employed in Publication IV was approximately 1 day. It should be noted that changes in the cell geometry and in the electrolyte composition, mainly the viscosity of the solvent, affect the time constant.

The segmented cell technique has some limitations: The studied materials must be freely moving in the electrolyte so that changes related to them may be seen in all the segments. In other words, if the adsorption of the studied material is much faster compared its diffusion, it adsorbs to the surfaces of the segment where it originates never reaching the other segments. For instance, according to Publication III, 4-*tert*-butylpyridine does not move freely but causes changes in the spatial performance distribution.

Another limitation is related to charge transfer: when current is driven through a segment, the electrolyte in the other segments may take part in the charge transfer process. This feature complicates comparison of the segmented cell performance to that of the small single cells. According to our measurements, this becomes a problem mainly in long measurements. If a segment is polarized for a long period of time, e.g. an hour, large visible changes in the electrolyte color due to the shift of I_3^- may be seen. The *i-V* measurements performed in the Publications III and IV were short, about 1 minute, which is why this effect did not impact the results. The reliability of the data could be confirmed, for instance, by changing the measurement sequence of the segments and checking that it did not affect the results.

3.2 Electrochemical Impedance Spectroscopy

In the EIS measurements, impedance components with different time constants appear at different frequencies and hence their response can be separated. In practice, the EIS measurements are carried out at an *i-V* point (DC) by applying a small amplitude alternating voltage to the test sample and measuring the current response. EIS spectrum is achieved by varying the frequency of the alternating voltage. In practice, the EIS spectrum shows the derivative of the selected *i-V* point (DC) divided to different components.

3.2.1   EIS analysis of solar dye cells

In EIS analysis, an equivalent circuit, which describes the different parts of the test sample with electrical components, is fitted to the measured EIS spectrum. The difficulty of the EIS analysis lies in the fact that an infinite number of circuits can be fitted well to an EIS spectrum. In order to get physically relevant data from the fitting, great care needs to be given to the construction of the equivalent circuit.

A complete equivalent circuit model of a DSC is illustrated in Figure 3.3. The model is similar to the one presented by Fabregat-Santiago et al. [20, 21]. In the circuit, constant phase elements (CPE) are used instead of pure capacitors since a CPE corresponds to a realistic electrode with an uneven and porous surface. A pure capacitor would describe a completely homogenous and even electrode surface. The equivalent circuit of a DSC shown in Figure 3.3 reduces to simpler circuits at different voltages as described in literature [20]. The different ways to understand the data at different voltages are discussed in Publications I and II.

The components of the equivalent circuit model presented in Figure 3.3:

- R_s is the ohmic series resistance caused mainly by sheet resistance of the substrates.
- CPE_{SU} and R_{SU} are the CPE and charge transfer resistance at the PE substrate/electrolyte interface.
- CPE_{CO} and R_{CO} are the CPE and charge transfer resistance at the PE substrate/porous TiO_2 interface. In Publication II, also the response caused by a blocking layer between the substrate and the porous TiO_2 layer are included in CPE_{CO} and R_{CO}.
- R_t ($= r_t d$) is the electron transport resistance in the TiO_2 layer and d is the thickness of the TiO_2 layer.
- CPE_{CT} ($= cpe_{CT}/d$) and R_{CT} ($= r_{CT}/d$) are the CPE and the charge transfer resistance at the TiO_2/electrolyte interface.
- Z_d is the mass transfer impedance at the CE due to ionic diffusion in the electrolyte.
- CPE_{CE} and R_{CE} are the CPE and charge transfer resistance at the CE/electrolyte interface.
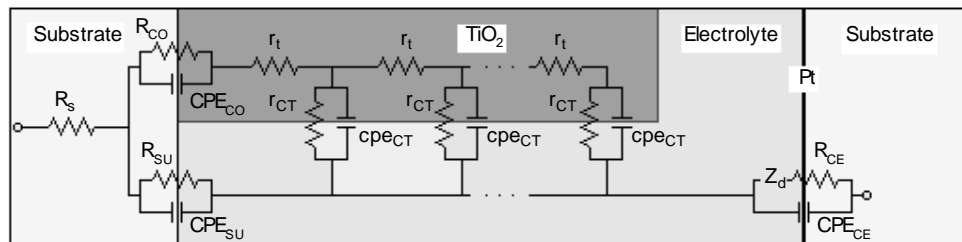
Figure 3.3   **A general equivalent circuit model of a DSC modified from the ones previously presented [20, 21].**

R_s, R_{CO}, R_t, Z_d, and R_{CE} impede the charge transport which relates to the proper operation of a DSC. In practice, they reduce the fill factor and thus also the cell efficiency. In a good DSC, these resistances are small. The recombination resistances R_{CT} and R_{SU} should on the contrary be as large as possible since they resist the current leakage from the PE to the electrolyte. A low recombination resistance decreases mostly V_{OC} which again results in losses in η.

The impedance spectra are usually plotted as so called Nyquist and Bode plots. In the Nyquist plot the real and imaginary impedance parts are plotted in a complex plane (Figure 3.4). The Bode plot shows the real and imaginary impedance as a function of frequency (Figure 3.5).

A typical DSC response at high negative voltages shows two arcs in the Nyquist plot (Figure 3.4) and two peaks in the Bode plot (Figure 3.5). Arcs and peaks refer to constant phase element – resistor -pairs. Commonly, the R_{CE} and CPE_{CE} pair results in one arc in Figure 3.4 and a peak in the kHz range as in Figure 3.5. R_{CT} and CPE_{CT} cause another arc (Figure 3.4) and a peak in the low frequency range at about 10 Hz (Figure 3.5). The electrolyte diffusion causes a Warburg element Z_d which shows in the mHz range [22] and it is overlapped by the R_{CT} and CPE_{CT} pair in Figures 3.4 and 3.5. The ohmic series resistance R_s does not have a capacitive component and therefore its value can be read directly from the real impedance axis at the high frequency end of the spectrum (Figure 3.4).

The effective electron lifetime τ_{eff} is useful quantity when studying recombination from the PE to the electrolyte. τ_{eff} can be determined from the frequency of the PE peak (Figure 3.5) with the following relation [22]:

$$\tau_{eff} = \frac{1}{2\pi f_{min}},$$
(4)

where f_{min} is the frequency of the minimum value of the PE peak. As the recombination increases, the PE peak moves to higher frequencies.
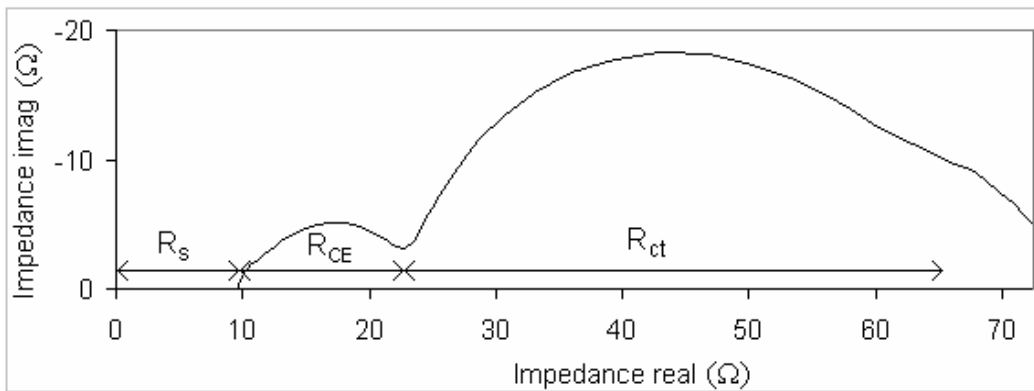
Figure 3.4   **Nyquist plot of a dye solar cell.**

23
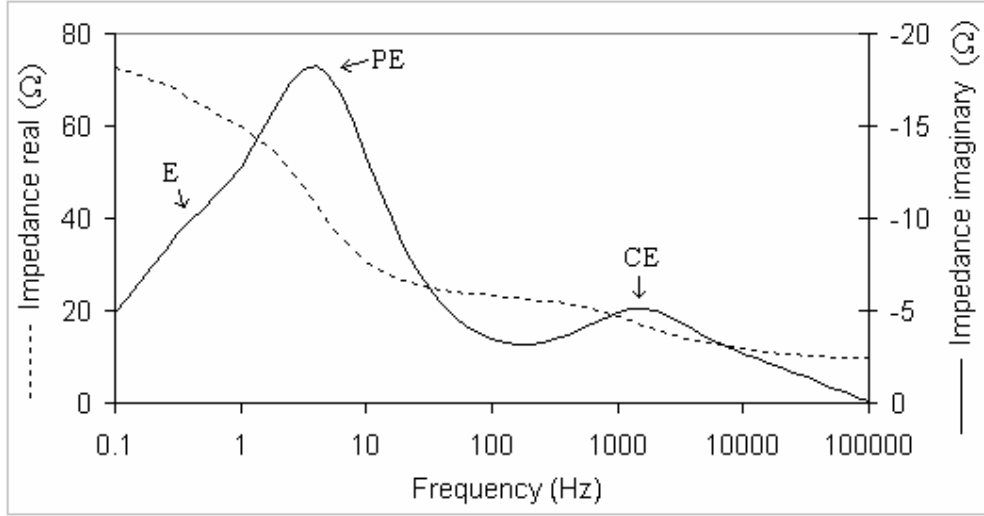
Figure 3.5   Bode plot of a solar cell. E = electrolyte, PE = photoelectrode, CE = counter electrode.

τ_{eff} can also be calculated from the PE equivalent circuit parameters [23]:

$$\tau_{eff} = (R_{CT} \cdot Q)^{\frac{1}{\beta}}. \tag{5}$$

where Q is the CPE$_{CT}$ pre-factor and β is the CPE$_{CT}$ exponent in the equation which describes the impedance of the constant phase element Z_{CPE}

$$Z_{CPE} = \frac{1}{Q \cdot (j \cdot \omega)^{\beta}}, \tag{6}$$

where ω is the angular frequency and j is the imaginary unit. Factor β takes into account the porosity and unevenness of a realistic electrode surface which results in dispersion in the R and C values. In the case of a pure capacitor, resistor - capacitor pair results in a perfect semi-circle which corresponds to situation in which β is 1. The dispersion of the values shows as flattening of the semi-circle in Nyquist plots such as in Figure 3.4. In practice β is regarded as an empirical factor and used only to improve fitting accuracy.

In addition to EIS, τ_{eff} can also be determined with transient techniques, such as open circuit voltage decay (OCVD) [15]. In the OCVD, the cell is first illuminated, then the light is switched off and the decrease of V_{OC} is measured. τ_{eff} can be calculated from the time derivative of V_{OC} with following equation [15]:

$$\tau_{eff} = -\frac{k_B T}{e}\left(\frac{dV_{OC}}{dt}\right)^{-1} \tag{7}$$

where t is the time, k_B is the Boltzmann coefficient, T is the temperature, and e is the elementary charge. The advantage of OCVD is that τ_{eff} can be obtained easily and quickly over large voltage range (Figure 3.6). τ_{eff} values determined with OCVD and EIS were found to have quite good comparability as can be seen from Figure 3.6b and as shown in Publication I.
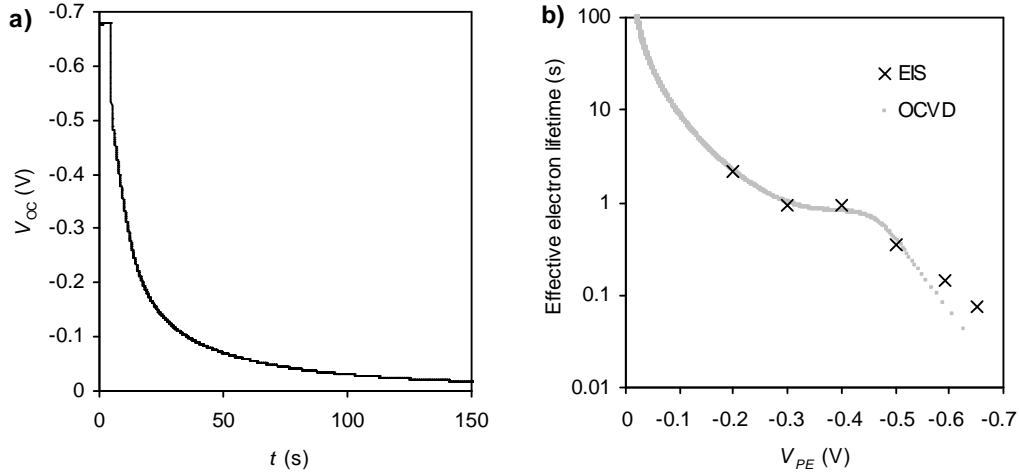
Figure 3.6   **a) The raw data of the OCVD measurement and b) τ_{eff} values determined with EIS and OCVD measured from a glass cell.**

3.2.2   Quantitative analysis of EIS response

The conventional way to make EIS measurements is under illumination at open circuit (OC). A downside of this method is that it gives the cell performance only at one point which does not give a comprehensive view of the cell performance. In addition, quantitative comparison of the recombination resistances at the PE/electrolyte interface in different cells is feasible only if they are compared in the same state meaning same V_{OC}. This is problematic since V_{OC} typically varies from cell to cell. Since R_{CT} depends exponentially on the voltage, even some tens of mV difference in V_{OC} will cause a clear difference in R_{CT}. That is to say, a direct comparison of R_{CT} in different cells with different V_{OC} leads to false conclusions. An example of a good cell and a poor cell may clarify this issue: The good cell has smaller recombination losses and higher V_{OC} than the poor cell. Due to the exponential dependence on the voltage, the EIS measurement at OC typically gives a larger R_{CT} to the lower V_{OC}. It would be erroneous to conclude that the cell with the smaller recombination resistance at OC would have higher recombination losses in general.

A more complete picture of the cell performance is gained if the EIS is measured as a function of voltage as shown in literature [20]. The measurements at different voltages

are commonly conducted in the dark as function of external voltage. Continuing from the same good cell – poor cell comparison, the good cell will more likely show a larger R_{CT} than the poor cell at a given voltage. When the comparison is made this way, the result is understandable: the good cell suffers less from the recombination losses.

The external cell voltage is divided differently between different cell components at different voltages. If a single cell component is examined, it should be studied as function of voltage over that particular component to gain quantitative comparison. The voltage over a single electrode can be calculated with the EIS data measured in a two electrode mode as first shown by Fabregat-Santiago et al. [21]. In Publication I, it is illustrated in detail how the polarization curve of a single electrode can be determined. The method is based on analyzing the EIS data as function of cell current instead of cell voltage. The voltage over a single electrode can also be measured with a proper reference electrode (three electrode measurement) [24, 25]. The application of such a reference electrode into a 20 μm thick cell is, however, very challenging.

4 Results and Discussion

The charge transfer at the different interfaces of the substrates is studied in Chapter 4.1. In Chapter 4.2, the study is expanded by studying the cell cross section layer by layer. In Chapter 4.3, the up-scaling issues are examined. Finally, in Chapter 4.4, stability analysis of the DSCs on StS is made.

4.1 Electrochemical Characteristics of Substrates

4.1.1 Charge transfer from the substrate to the electrolyte (Publications I and II)

Depending on which electrode is prepared on the substrate, either a very small or very large charge transfer resistance between the substrate and the electrolyte is desired. In the case of a CE, a small charge transfer resistance at the substrate would be preferred. If the resistance is small enough, no catalyst layer is needed on the CE substrate. This is, however, rarely the case and a catalyst layer is required to reach low charge transfer resistance at the CE. For instance, Toivola et al. reported R_{ct} of 10^{13} $\Omega \cdot cm^2$ for plain StS CE while a properly working CE should result in R_{ct} about 10 $\Omega \cdot cm^2$ [8].

Contrary to the situation at the CE, a large charge transfer resistance at the PE substrate /electrolyte interface R_{SU} is needed to minimize the current leakage i.e. recombination from the substrate to the electrolyte. In Publication I, the electron recombination from the StS PE substrate was studied and it was shown to be approximately an order of magnitude smaller than that from the FTO-glass substrates. Hence, in regard of recombination StS is a better PE substrate compared to FTO-glass. In Publication II, the recombination from ITO-PET substrate was detected to be similar to that from FTO-glass.

The effect of the recombination from FTO-glass on η is typically insignificant at high light intensities (~1 sun) [26, 27]. In Publication II, this result was again confirmed for FTO-glass and shown to apply also for ITO-PET. Logically, the same should apply for StS as well, because of the even lower leakage current compared to FTO-glass.

Previously, thin (1-200 nm) compact TiO_2 blocking layers have been made typically with spray pyrolysis or sputtering [26-29]. In Publication II, a new method for the blocking layer preparation, atomic layer deposition (ALD), was tested in the preparation of compact TiO_2 layers. At low light intensities, recombination was detected significant for both FTO-glass and ITO-PET; for instance, 4 nm ALD TiO_2 layer on ITO-PET increased V_{OC} 50 % at low light intensities as Figure 4.1 indicates (Publication II). Similar results have been reported in literature for FTO-glass based cells [26, 27].
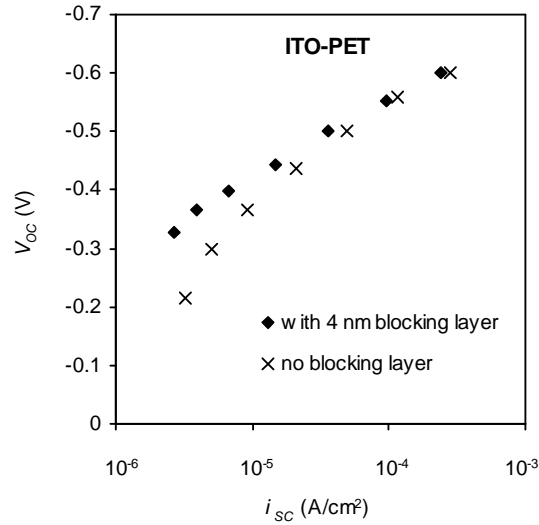
Figure 4.1 V_{OC} **as a function of** i_{SC} **in the ITO-PET cells with and without a recombination blocking layer. Data is from Publication II.**

In conclusion, the use of blocking layers does no appear to be beneficial in outdoor applications, such as in roofing or façades, which are typically exposed to quite high light intensities. In indoor applications on the other hand, the blocking layers appear to be very useful. Note that the results presented above are gained with a standard liquid type electrolyte and the recombination from the substrate has been reported to be larger in the cells filled with ionic liquid electrolyte [30].

4.1.2   Charge transfer from the substrate to the other electrode components (Publications I and II)

Efficient charge transfer from the substrate to the other parts of the electrode is important but seldom discussed characteristic. In Publication II, the charge transfer resistance at the high frequencies was multiple times larger in the case of DSCs with ITO-PET substrate and also with some of the blocking layers compared to that in normal glass cells. The enlarged resistance was attributed namely to the presence of the charge transfer resistance between the substrate and the porous TiO_2 layer R_{CO}. In some cases at high light intensities, the use of a blocking layer resulted in a larger negative effect due to increased R_{CO} compared to the positive effect caused by the smaller recombination as presented in Publication II. Hence, it is advisable to examine R_{CO} in particular when studying the influence of a blocking layer.

The detection of R_{CO} is not as straightforward as that of other DSC impedance components: Firstly, in Publication II as in the previous ones [21, 31], R_{CE} overlapped R_{CO}. Without a duly quantitative comparison, the presence of R_{CO} could have not been
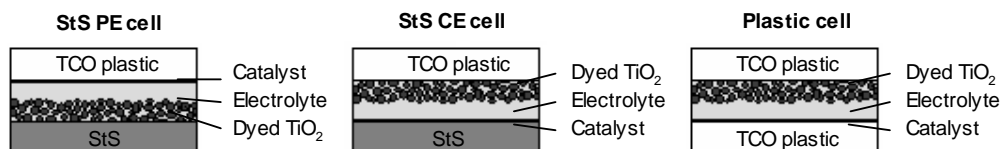
confirmed in any of these studies. Secondly, R_{CO} was not a constant but changed significantly as a function of current (and voltage) (Publication II). In practice, if EIS measurements are made only at one high voltage, such as under illumination at V_{OC}, R_{CO} might be too small to be seen and thus easily missed even if it would be highly significant at smaller voltages. Hence, it is good to make several EIS measurements as function of voltage (or current) and compare the studied impedance component as a function of current as suggested in Publication I and illustrated for the charge transfer at high frequencies in Publication II to quantitatively decouple separate the effects caused by different cell components.

Only the charge transfer at the PE was considered above. In principal, similar charge transfer problems could also occur at CE between the substrate and the catalyst. Such interfacial resistance might explain, for instance, why thermally platinized StS CE has poorer performance compared to similarly prepared FTO-glass CE (data presented in Publication I).

4.2 Optimization of Cell Structure

The structures of the different types of flexible DSCs are presented in Figure 4.2. DSCs with CE on stainless steel (StS CE) and DSCs completely on plastics are illuminated so that the light comes directly to the PE, similar to the situation in the conventional glass cells. These cell types are hereafter called as the PE illuminated cells. The cells with a non-transparent PE substrate, to which the light comes through the CE, such as the StS PE cells, are referred to as the CE illuminated cells.

The optimization of the PE and the CE illuminated cells differs greatly. For instance, in the former case an opaque CE can be used whereas in the latter case a transparent or at least a semi-transparent one is required. The characteristics and optimization of the CE catalyst layer, the electrolyte, and the dyed TiO_2 layer are discussed in Chapters 4.2.1-4.2.3. Although, the optimization of the TiO_2 layer thickness was not examined in the Publications, the issues affecting it are briefly discussed in Chapter 4.2.3 for the sake of completeness. Here, the optimization focuses on the CE illuminated cells since the optimization of the PE illuminated cells has been studied widely in the literature, in fact the majority of the publications about DSCs aims to improve the standard type PE illuminated glass cells.

StS PE cell	StS CE cell	Plastic cell
TCO plastic — Catalyst	TCO plastic — Dyed TiO_2	TCO plastic — Dyed TiO_2
— Electrolyte	— Electrolyte	— Electrolyte
StS — Dyed TiO_2	StS — Catalyst	TCO plastic — Catalyst

**Figure 4.2**   **The structure of a StS PE cell, a StS CE cell, and a plastic cell.**

The study of the performance of the CE, the electrolyte, and the PE were all found important: The charge transfer in the TiO_2 was particularly important in those PEs prepared with low temperature methods as shown in Publication II. For the StS PE and the standard glass cells prepared for Publication I, it was calculated that the losses caused by R_{CE}, Z_d, and R_s were of similar magnitude, and further action should be taken to reduce them all. Interestingly, the sum of R_{CE}, Z_d, and R_s remained approximately constant as a function of cell current. This is because the changes in the values of R_{CE} and Z_d canceled each other out: when increasing the current through the cell, the losses caused by R_{CE} decreased whereas losses by Z_d decreased. As a result, the combined effect of R_{CE}, Z_d, and R_s to the i-V curves did not differ from that of large R_s. This is an important issue to realize also in the preparation and validation of DSC models.

4.2.1   Counter electrode catalyst layer (Publications I and VI)

The most important characteristic of a good catalyst layer is a small charge transfer resistance from the CE to the electrolyte, R_{CE}. Commonly used high performance catalyst materials are Pt and carbon black. Indeed, the highest StS CE cell performance (9.15 %) has been reached with carbon black as catalyst layer [33]. In the CE illuminated DSCs, such as the StS PE cells, high enough transmittance of the CE is equally important. For instance, porous carbon black catalyst layers cannot be used in the CE illuminated cells, because they are practically non-transparent.

In Publication VI, a series of different semi-transparent catalyst layers for the CE illuminated cells were tested. The studied catalyst materials were Pt and conducting polymers PEDOT-TsO and PEDOT-PSS and they were deposited using different methods. Optimization was done between the transmittance and the efficient charge transfer since typically a decrease in the catalyst layer thickness improves the former but decreases the latter. In Publication VI, the highest η of the CE illuminated cells was reached with 2-3 nm layer of sputtered Pt. It may be possible to reach even high performance by decreasing the sputtered Pt layer even further. PEDOT-TsO resulted in quite good catalytic activity as well. The differences in R_{CE} with the different layers show clearly in the i-V curves (Figure 4.3): with PEDOT-PSS the i-V curve was quite flat near OC whereas with sputtered Pt and PEDOT-TsO it was much steeper. Hence, η of the PEDOT-TsO cells was in fact more than 50 % lower compared to the others. The performance of the polymer catalysts is in agreement with the literature [34].

The best deposition method depends both on the catalyst material and on the substrate: For instance regarding the application of PEDOT-TsO, a thick, almost non-transparent film was needed with spraying to reach the same R_{CE} achieved with a thin, highly transparent thin film prepared with spin-coating (Publication VI). In Publication I, it is shown that the StS CEs prepared with thermal platinization gave large R_{CE} whereas for glass cells the technique is regarded as one of the best. R_{CE} of StS CE cells was in fact so large that it resulted in s-shape curvature near the open circuit in the i-V curves (Figure S3 in Publication I), which is typical for a large R_{CE}. The s-shape curvature can also been seen in Figure 4.3 and in Publication VI in the DSCs with no catalyst layer.
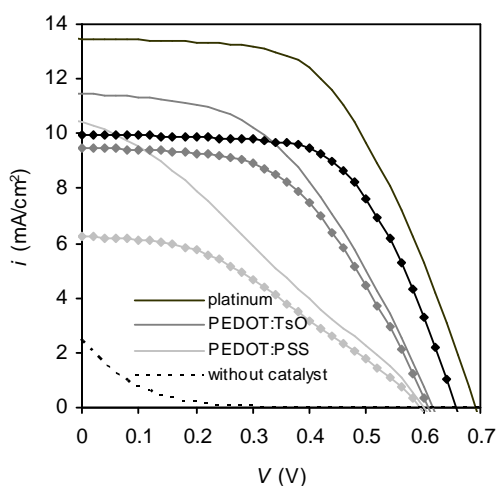
Figure 4.3 *i-V* **curves of DSCs with glass PE and ITO-PET CE with different catalyst layers. The straight lines refer to PE illumination and the dotted lines to CE illumination. Data is from Publication VI.**

The catalyst layer must also be properly attached because detached catalyst particles may form recombination centers in the TiO_2 layer. In Publication VI, the physical attachment of PEDOT-TsO was detected to be poorer compared to sputtered Pt in tape tests. The DSCs with PEDOT-TsO had lower V_{OC} and i_{SC} compared those with sputtered Pt (Figure 4.3). Since the differences could not be explained with optics or R_{CE}, the catalyst layer had presumably contaminated the TiO_2 layer.

4.2.2   Electrolyte (Publication VI)

The resistance Z_d caused by diffusion of the electrolyte at the CE contributes to the fill factor losses. Since I_3^- ions in the electrolyte absorb light in the wavelength range less than 500 nm, the electrolyte causes also optical losses [35]. The other electrolyte components used in this work are practically transparent at least in the wavelengths of visible light. In the PE illuminated cells, some of the incident light is absorbed by the electrolyte in the pores of the TiO_2 layer. In the CE illuminated cells, there is also the bulk electrolyte layer causing optical losses. Therefore, the losses by the electrolyte and also the need for optimization are much greater in the case of the CE illuminated cells compared to the PE illuminated cells.

The optical losses caused by I_3^- in the electrolyte are to some extent dependent on the current passing through the cell. This is because the local concentration of I_3^- depends on both the applied current and the distance from the electrode. In practice, when increasing the cell current, a larger part of I_3^- moves from the bulk electrolyte layer to the TiO_2 film [36]. The shift of I_3^- in the working conditions decreases the optical losses

in the CE illuminated cells whereas in the PE illuminated cells the optical losses increase.

The two easiest ways to decrease the amount of I_3^- shadowing the PE are to decrease the bulk electrolyte layer thickness and to lower the I_3^- concentration as shown in our previous work [37]. The reduction of the bulk electrolyte is in general beneficial since it eases the mass transport in the electrolyte. The reduction of I_3^- concentration is by contrast restricted since there needs to be enough I_3^- to transport the current in working conditions. When the concentration of one charge carrier species goes to zero at one electrode, the current through the cell cannot be increased further and thus the limiting current is reached. The limiting current i_{lim} of DSCs is proportional to the distance between the electrodes l, the diffusion coefficient of I_3^- D_{I3-}, and the concentration of I_3^- c_{I3-} [38]:

$$i_{lim} = \frac{2nFD_{I3-}c_{I3-}}{l} \tag{8}$$

where n is the number of electrons transferred in each reaction (here 2), and F is the Faraday constant. In practice, the limiting current should be at least about 50 % higher compared to the cell current in working conditions in order to have efficient charge transfer in the electrolyte. With this kind of simple adjustments in the bulk electrolyte layer thickness and in I_3^- concentration, i_{SC} was increased by 15 % in the StS PE cells as shown in Figure 4.4.

A more exotic way of reducing the electrolyte color, bleaching, was tested in Publication VI. The idea in bleaching is to convert the highly absorbing I_3^- ions to colorless IO^- ions with a base [35]. Although the bleached electrolyte had high transparency, the charge transfer reactions slowed down to the extent that the net result in the efficiency was negative as described in more detail in Publication VI.
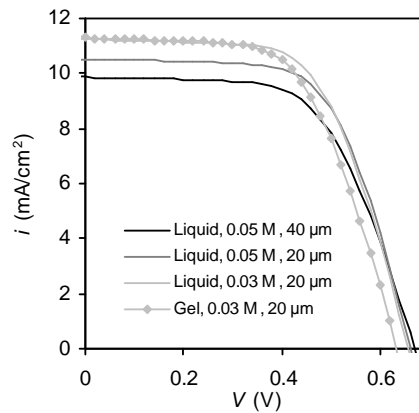
Figure 4.4 *i-V* curves of glass solar cells with different I_3^- concentration in the electrolyte and distance between the electrodes in CE illumination.

In addition to the performance, also the stability and safety of the electrolyte need to be taken into account in the designing of the electrolyte. The solvent used in this work, 3-methoxypropionitrile, is known as more robust [39] and also less toxic compared to other commonly used alternatives such as acetonitrile. A hazard related to the DSCs is that electrolyte may leak out of the cell in the case of a physical breakage. By using gel and ionic liquid electrolytes instead of liquid electrolytes, this may be prevented. As noted in Publication VI and described also in Figure 4.4, gelling of the electrolyte reduced V_{OC} about 20 mV, but optically the gel and liquid electrolyte were very similar resulting in equal i_{SC}. The viscosity of the ionic liquid electrolytes is much higher than of normal liquid and gel electrolytes and hence the charge transfer is not as efficient. To gain sufficiently high i_{lim} with ionic liquid electrolytes, I_3^- concentration needs to be very high. This increases optical losses in particular in the CE illuminated cells. Hence, if the ionic liquid electrolytes do not additionally improve some other cell characteristics such as lifetime, gelling is a better option to the mechanically stabilize the electrolyte in the CE illuminated cells.

4.2.3   Dyed TiO$_2$ layer (Publication II and VI)

The light absorption in the dyed TiO$_2$ films follows the Beer-Lambert law which means for the normal PE illuminated cells that the amount of photons absorbed by the film decreases as the distance from the PE substrate increases. In other words, the light absorption in the PE illuminated cells is largest near the PE substrate. The situation is the opposite in the CE illuminated cell in which the light absorption is the smallest near the PE substrate. The closer the electrons are injected to the PE substrate, the higher is the probability of electron collection. Hence, light absorption near the PE substrate, as it is with the PE illuminated cells, is preferable. If the TiO$_2$ film is of very good quality meaning that electron lifetime τ_{eff} is long, electron collection should not be a problem even if the electron is absorbed and injected far from the PE substrate. Typically sintered TiO$_2$ films have good characteristics.

Current collection is, however, a significant issue in the case of the low temperature treated PE, such as those made on plastic. Typically the necking of the TiO$_2$ particles is not as good with low temperature methods which results in poorer performance as shown in Publication II. The issues related to the electron collection in the low temperature pressed films has been discussed in detail by Halme et al. [32]. With optimization of the TiO$_2$ particle size, the solvent, and the treatments for the low temperature treated TiO$_2$ film respectable 7.4 % cell efficiency has been achieved [40].

The light absorption is often increased by reflecting the light back to the photoactive layer after it has once passed though it. In the glass and plastic cells, this can be done, for instance, simply by placing a back reflector such as a mirror behind the cell. In the StS cells, the StS substrate serves as a back reflector [11, 41]. In the glass cells, the back reflector is most commonly integrated to the TiO$_2$ layer by using two different kinds of TiO$_2$ layers [4]: the first layer has low reflectance and the second one high reflectance so that the second layer reflects the light back to the first layer.
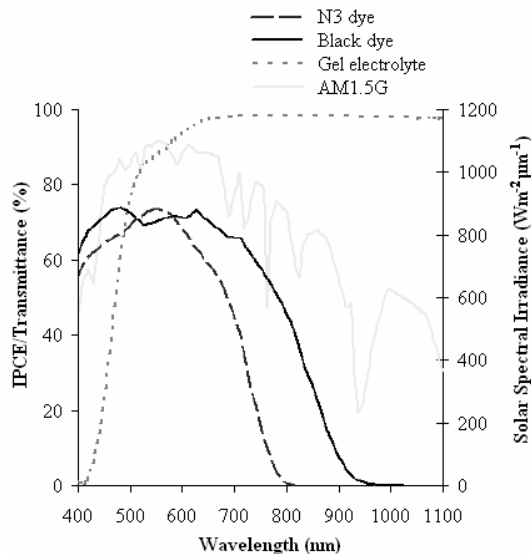
Figure 4.5 IPCE spectra of the black and the N3 dyes [42], transmittance of the electrolyte, and AM1.5G solar spectral irradiance. Data is from Publication VI.

The differences in the light direction affect also the selection of the dye: The CE illuminated cells cannot utilize the low wavelengths efficiently due to high absorption by the electrolyte in that spectral range (Figure 4.5). However, in the high wavelengths, there are practically no optical losses by the electrolyte (Figure 4.5). Thus, it would be convenient to improve the utilization of the high wavelengths in the CE illuminated cells (Publication VI). This could be done, for instance, by using a black dye (Figure 4.5) instead of commonly used red dyes, such as N3 (Figure 4.5) and N-719. The black dye does not, however, adhere to the TiO_2 layer as efficiently as the red dyes [43] and to reach the same amount of injected electrons, a thicker TiO_2 layer is required in the case of the black dye compared to the red dyes. In the CE illuminated cells, the increase of the TiO_2 layer thickness results in that the electrons are injected on average even further from PE substrate which may cause problems in the electron harvesting.

4.3 Scaling Up

A few demo DSCs with a larger area (substrate size 6×6 cm) were prepared during this thesis work although they were not included in the Publications of this thesis. A demo cell with StS PE and plastic CE is presented in Figure 4.6. In further tests conducted mainly by others in the group, some changes were made to the demo cells; the largest change being that the silver stripes for the current collection on the plastic CE were printed instead of handmade as in the cell in Figure 4.6. 3.4 % efficiency was achieved for the demo StS based DSC in the further tests [44]. In those tests, the electrolyte contained 4-*tert*-butylpyridine which was shown in Publication III to cause spatial performance losses when the standard filling method was used. Hence, by changing the

34

electrolyte composition or the filling method, even higher performance than that reported in [44] should be reached. Next, current collection and spatial performance distribution are discussed more.

4.3.1 Current collection

Current collection is a common problem in the up-scaling of solar cells. The width of a single conventional DSC is restricted to approximately 1 cm due to the high sheet resistance of TCO layers (~10 Ω/Sq.) [45]. In other words, to increase the cell/module size, current collectors need to be placed 1 cm apart from each other. The current collectors shadow the cell and thus decrease the active area. The effect of the silvery current collectors to the active area can be seen in Figure 4.6. The optimization of the current collectors is analyzed in detail by Toivola et al. [44].

With sheet resistance of StS (~0.003 Ω/Sq. [6, 7]), the width of a single cell could easily be above 10 cm. In the StS based cells, current collectors are still required for the transparent electrode with the TCO layer as indicated also in Figure 4.6. The cell preparation and the encapsulation would be significantly easier if current collectors were not needed inside the cell at all. In the future, breakthroughs in nanotechnology may lead to substantially higher conductivity of TCO layers.

Although the metal substrates are convenient since current collectors are not required on them, there are problems in the series connection of these cells. In practice, the series connection of a metal based DSC is impossible without cutting the substrate whereas in the cells based completely on TCO coated substrates, it is sufficient to cut only the TCO layer to form the series connection. If the series connection is not made, the voltage of the module is limited to that of a single cell (V_{OC} is typically about 0.6-0.8 V). Most practical applications require much higher voltage than that and an up-converter is needed.


Figure 4.6 Example of a StS DSC with a larger active area.

4.3.2   Spatial performance distribution (Publication III)

In addition to the conventional up-scaling problems with current collection discussed above, spatial performance distribution may also cause significant losses. In Publication III, a segmented cell design was introduced to analyze the spatial distribution of all the photovoltaic characteristics. There was a clear variation, about 10-20 %, not only in i_{SC} but also in V_{OC} (Publication III).

The even decrease of V_{OC} along segmented cell led to the hypothesis that the effect could be connected to the electrolyte filling as described by Figure 4.7. The hypothesis was found correct since the cell performance could be manipulated by changing the position of the electrolyte filling hole (Publication III). The problem was further linked with the uneven adsorption of 4-*tert*-butylpyrine, a common additive in DSC electrolytes, in the filling process (Publication III).

The performance loss due to the uneven spatial distribution was highly significant since in the case of a 4-segment cell with an active area of 1.2 cm^2, the efficiency loss due to the spatial effects was already 20 % (Publication III). To improve the performance of large area DSCs, it is essential to eliminate these losses. Since the spatial variation was connected to the electrolyte filling and a certain electrolyte component, the study of the alternative electrolyte filling methods and/or electrolyte compositions is called for.
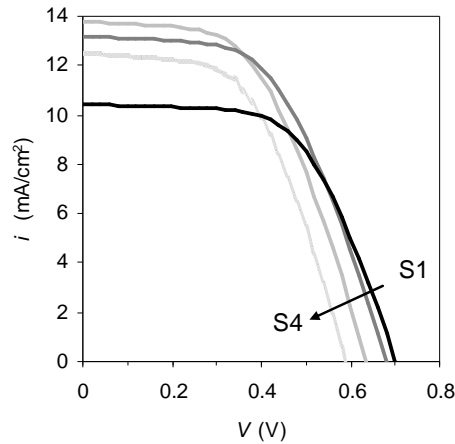


Figure 4.7 *i-V* curves of the different segments in a 4-segment cell. The segment nearest to the electrolyte filling hole is marked with S1. The other segments are numbered consecutively towards the other end of the cell. The numbering order is indicated with the arrow.

4.4   Stability of Stainless Steel Based Dye Solar Cells

Since high efficiencies can be reached with flexible DSCs (record 8.6 % [13]), the focus of the study should be turned to the lifetime of the cells. In the Publications I and IV-VI, the stability of the StS based DSCs is examined. The lifetime analysis of the plastic substrate was not included in this work. It is, however, an important subject for the development of flexible DSCs and hence it should be examined in further studies.

Considering the stability of StS substrates, the passing of the electrolyte soaking tests [6-8] is only a basic stability requirement and as such it does not prove the stability of the complete DSC based on StS. Indeed, the StS based DSCs showed poorer stability compared to the glass based cells as noted in Publications IV-VI, see also Figure 4.8. The instability of the StS CE cells has been mentioned in literature and there it was linked to sealing problems [6]. It has also been suggested that StS cells might be subject to corrosion [33] and that StS PE substrate may result in significant leakage current [11]. Furthermore, it has been recommended to retain from contacting DSC components with metals to avoid possible surface contamination of PE TiO_2 layer by harmful metal oxides [46]. On this ground, preparing DSCs on metals contains many questions. In this contribution electrochemical and spectroscopic analyses of the StS based DSCs is made to clarify these issues.

The initial state (Figure 4.8, A) of the StS cells was studied in Publication I and in Chapter 4.4.1. The stability related to the initial state covers the reactions from the cell preparation to the first measurements. The rapid degradation of the StS PE cells (Figure 4.8, B) was examined with the novel segmented cell method in the Publication IV (Chapter 4.4.2). In Publication V, it was found that the StS CE cells are not stable either, and their aging was linked with corrosion (Chapter 4.4.2 and Figure 4.8, C).
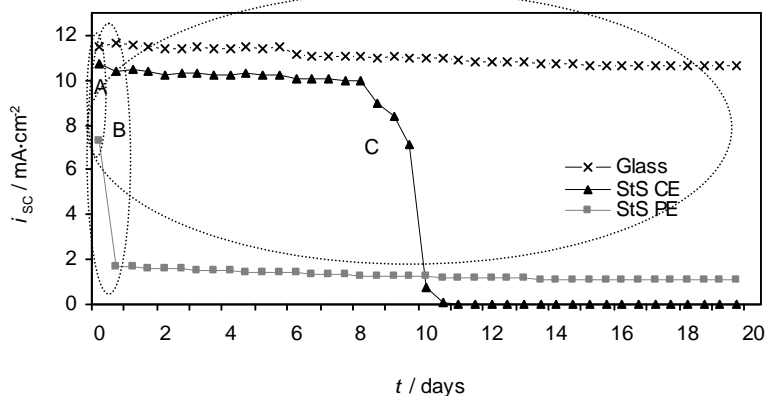

Figure 4.8 i_{SC} as function of time in typical StS PE, StS CE, and glass cells. The ovals marked with letters A-C refer to different phases in the degradation. Part of data is from Publication V.

37

4.4.1　Initial stability (Publication I)

In Publication I, the initial performance of StS based cells and the effect of the stainless steel to other cell components was examined. In order to perform quantitative comparison of the components, a method to calculate a single impedance component *i-V* curve on the basis of the whole cell EIS response was needed. It should be noticed that if the EIS data would have been analyzed in the commonly used way i.e. as function of external cell voltage, it would have resulted in different, erroneous, conclusions.

With the calculations explained in detail in Publication I, it could be determined that the StS PE substrate increased the recombination current from the dyed TiO_2 layer (Figure 4.9). Interestingly, the StS CE did not affect the initial performance of the PE. The mechanism through which the StS PE substrate affected the TiO_2 layer is still unclear. StS substrate affecting other cell components can either refer to a steady characteristic or, as more likely, to arising stability problem.

The possibility that the StS might cause surface contamination to the TiO_2 layer with metal oxides, such as iron oxide forming recombination centers as suggested in literature [46], was investigated in Publication I. A direct evidence of surface contamination of TiO_2 layer by a contact to a metal object has not been presented in literature. In Publication I, some glass PEs were pressed against StS during the sintering to cause surface contamination. Their performance did not, however, differ from the normally made glass DSCs indicating that there was not at least significant surface contamination. In addition to that, the i_{SC} values of the StS cells were equal to those of the glass cells when illuminated from same direction which also implies that there is no contamination by the StS cells that would affect the photovoltaic performance (Publication I). Note that these contamination tests apply only for the initial state.
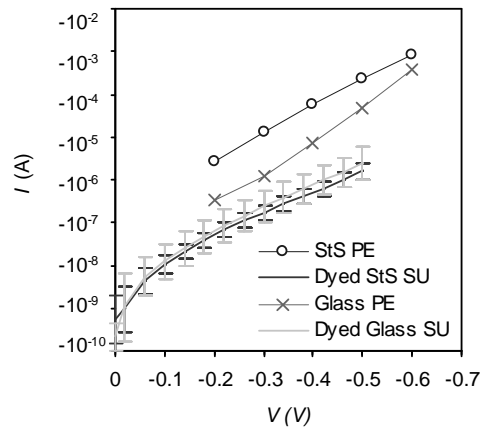
Figure 4.9 Polarization curves of StS PE and glass PE calculated based on EIS data and measured curves of dyed StS substrate and dyed glass substrate. Error bars indicate the standard deviation and they are shown when larger than the marker size. Data is from Publication I.

38

4.4.2   Fast degradation (Publication IV)

The StS PE cells were subject to very fast degradation: in a few hours under illumination the StS PE cells experienced about 80 % loss of i_{SC} (Publication IV). The StS PE cells were sealed similarly to the StS CE cells which remained stable that period of time. Hence, the aging of the StS PE cells could not be due to insufficient sealing.

There were no visual changes in the StS PE cells that would correspond to this performance loss (Publication IV). For instance, in the case of corrosion, I_3^- typically reacts with the metal resulting in a clear color loss in the electrolyte [6, 8]. The SEM and EDS analyses showed changes neither in the surface structure nor in the composition of the StS PE (Publication IV). These results imply that the aging of the StS PE cells was not due to corrosion either.

Both OCVD and EIS measurements indicated increased recombination from the StS PE (Publication IV). This led to the hypothesis that the aging of the StS PE cells might be due to contamination of the TiO_2 layer. Note, that SEM and EDS cannot detect small quantities of small particles (diameter less than 1 nm) and the contamination tests presented in Publication I apply for the initial state only. Thus, based on these tests the possibility of contamination cannot be completely excluded.

To further analyze the mechanisms leading to the StS PE cell degradation and the possibility of contamination, segmented cell design was developed for aging studies in Publication IV. In the segment cell tests, the focus was on the participation of the electrolyte to the aging process. The idea in the segmented cell tests was that if there were significant changes in the electrolyte during the aging of the StS PE cells, they should transfer from a StS PE segment to the reference glass segment as explained in Publication IV and Chapter 3.1.2. The performance of the reference glass segmented was compared to that of 2-segment cells composed of two glass segments. No changes in the reference glass cell could, however, be detected (Publication IV).

The adsorption of the contaminating material in the StS PE segments might, however, prevent it from occurring in the reference glass segment. To study this possibility, the probability of the adsorption was reduced by decreasing the amount of active area in the StS segment. In practice, the large surface area TiO_2 photoelectrode film was left out of the StS segment. To mimic the DCS performance, the dyed StS substrate was polarized. The polarized StS substrates did not affect the glass segment either.

The two different segmented cell tests both indicate that the electrolyte was neither contaminated nor was subjected to other significant changes that would itself cause the rapid degradation of the StS PE cells. Interestingly, according to the Publications I and IV, the degradation of the StS PE cells was not due to any of the reasons suggested in the literature [6, 11, 33, 46]. Thus, further work is needed to determine the mechanisms leading to the short lifetime of the StS PE cells.

4.4.3 Slow degradation (Publication V)

The lifetime of the StS CE was considerably longer compared to the StS PE cells as noted in Publications IV and VI and as illustrated in Figure 4.8. The StS CE cells show, however, much poorer stability compared to glass cells (Figure 4.8). A steady decrease in the performance of StS CE cells has been reported in literature [6], and the effect was suggested to be caused by insufficient encapsulation. Contrary to that, here the StS CE cells were completely stable for about a week, but after the stable period the cells suffered from a rapid degradation affecting mostly i_{SC} (Publication V). In addition to the decrease of i_{SC}, a simultaneous loss of electrolyte color was detected and it was followed by formation of black spots in the cell (Publication V).

The aging of the StS CE cells was linked with general corrosion (Publication V): Firstly, the color loss of the electrolyte is typical for metal corrosion in DSC electrolyte [6, 8]. Secondly, SEM analysis revealed presence of evident corrosion pit holes on the StS CE substrate (Figure 4.10). Thirdly, EDS elementary analysis proved that the black spots on the PE of the StS CE cells were composed of StS metals and iodine, and hence they were apparent corrosion residues.

To stabilize StS CE cells, a corrosion protection layer is needed. Alternatively, the electrolyte composition could be changed to less aggressive; for instance, some solid state polymer electrolytes could be suitable.
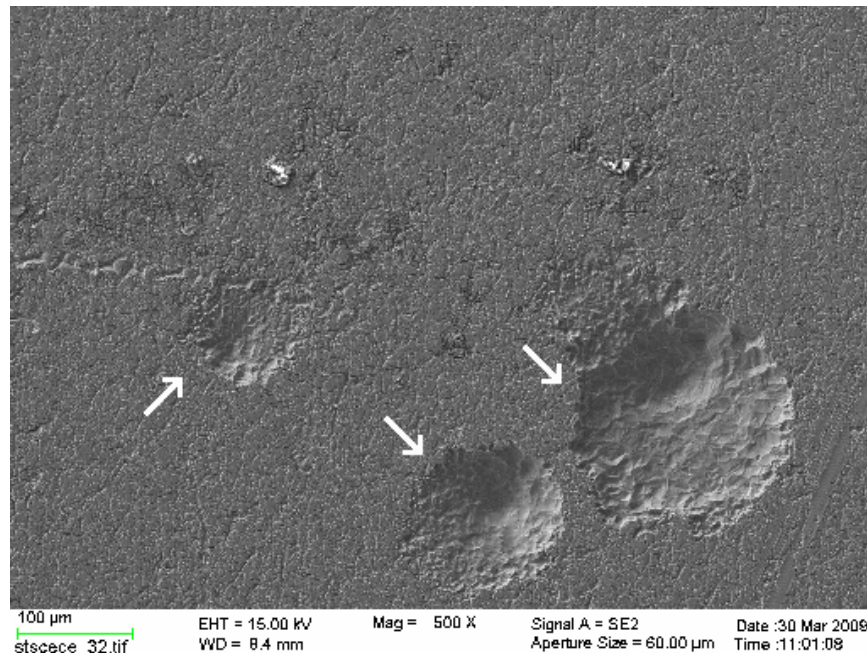
Figure 4.10 SEM image of the surface of the aged StS CE. The pit holes are marked with arrows.

5   Conclusions and Summary

In this thesis, the technological aspects related to the production of larger area flexible dye solar were examined to find the factors that limit the performance and stability. The study is centered around the substrate. First, electrochemical characterization of the substrates was made. Second, optimization of the other cell components in the different cell configurations were examined taking into account the restrictions that the substrates cause (direction of light, limitations in the temperature treatments etc.). Third, up-scaling issues i.e. current collection, focusing on differences between metal and TCO substrates, and uneven performance distribution were studied. Fourth, the stability issues related to the cells based on stainless steel substrates were examined.

The largest problems were seen in the area of stability: The aging was serious in the dye solar cells with stainless steel photoelectrode as they degraded in a matter of hours under illumination. The dye solar cells with stainless steel counter electrode suffer from insufficient stability as well, since the cell lifetime was only about a week under illumination.

In the case of stainless steel counter electrode cells, there were multiple changes that related the aging of the stainless steel counter electrode cells to general corrosion: the loss of electrolyte color indicating loss of tri-iodide, pit holes on the StS that are typical for corrosion, and apparent corrosion residues on the PE. Contrary to the stainless steel counter electrode cells, the mechanisms resulting in the degradation of the stainless steel photoelectrode cells remain unclear. According to visual observations as well as SEM and EDS analyses, there was no corrosion in the stainless steel photoelectrode cells. The initial studies as well as the later segmented cell studies showed no sign of contamination either. With segmented cells, it could be also determined that there were no changes in the electrolyte that would cause the aging. Thus, the systematic analysis of the stainless steel photoelectrode cells needs to be continued to determine their degradation mechanisms.

Significant problems were found also in the field of up-scaling. A previously unknown loss factor affecting the whole DSCs research field, spatial performance distribution occurring in the electrolyte filling, was discovered in this work. A novel segmented cell configuration was introduced to acquire spatially resolved *i-V* data. The spatial distribution losses are very important as in a small cell with active area of 1.2 cm^2 the losses by the uneven 4-*tert*-butylpyridine distribution were already 20 %. Since the spatial distribution problems were detected to be related to a specific filling method and an electrolyte component, alternative filling methods or electrolyte compositions are logical areas of future study.

Both StS and ITO-PET are at least as good substrates as FTO-glass regarding recombination, and for high light intensity applications no blocking layers are needed on either of them. If the cells are designed to operate mainly at low intensities such as indoors, a blocking layer is useful in increasing the cell voltage, for instance the 4 nm TiO$_2$ layer on ITO-PET increased V_{OC} even as much as 50 % at very low light

intensities. The performance of the blocking layer may even improve if the thickness is reduced. A thinner layer would also be better in regard to manufacturing as the preparation time would be shorter.

Good low temperature counter electrodes and electrolyte compositions to be used in the counter electrode illuminated cells, e.g. stainless steel photoelectrode cells, were found. The preparation of low temperature TiO_2 layer for plastic photoelectrodes still has room for improvement.

The thesis also produced achievements in the methodological side, namely by the introduction of the segmented cell design and by the presentation of how to reach quantitative EIS analysis. The purpose of both segmented cell method and EIS is to decouple the effect of different cell components on the cell performance. Both methods are non-destructive and therefore they can be used also for continuous examination of the cell performance. The theoretical principles of the techniques are very different and therefore they are largely complementary as indicated in Publication V.

The quantitative method to analyze EIS data as a function of cell current was presented and the conventional methods were shown to be insufficient and even misleading. By employing this technique, it could be determined that the StS PE substrate had increased the recombination from the PE while the StS CE had not. The effect could not be caused by the increased recombination from the substrate since the recombination losses from the StS PE substrate are smaller compared to those from conventional TCO glass substrate. Hence, the StS PE substrate appears to have affected the dyed TiO_2 film.

The segment cell method was useful since it provided spatial distribution data of all the photovoltaic parameters whereas the previous techniques showed only the distribution of the photocurrent. Hence, it could be directly calculated how large the losses are that the spatial distribution causes to the cell efficiency. The segmented cell method for aging studies is a good technique for the examination of those degradation effects that are transmitted by the electrolyte. In Publication IV, the reactions with the electrolyte and stainless steel substrate were examined. The same principles can be used for several other aging problems, such as dye desorption.

In conclusion, one of the most critical issues related to the flexible dye solar cells is the stability as reaching high cell performance with flexible DSCs substrates is not a problem anymore. In regard to stainless steel based cells, a longer cell lifetime is needed. In the case of the cells with stainless steel photoelectrode, continuing the systematic analysis to determine the aging mechanisms might be the best way to solve the degradation problem. As the mechanism causing the aging of the stainless steel counter electrode cell is known, the next step is to find a suitable protective layer or an electrolyte composition to avoid the corrosion. An important issue is also the determination of the lifetime of the plastic electrodes. More aging studies in the DSC field are in general needed and the segmented cell design will be useful in the examination of cell degradation in the future.
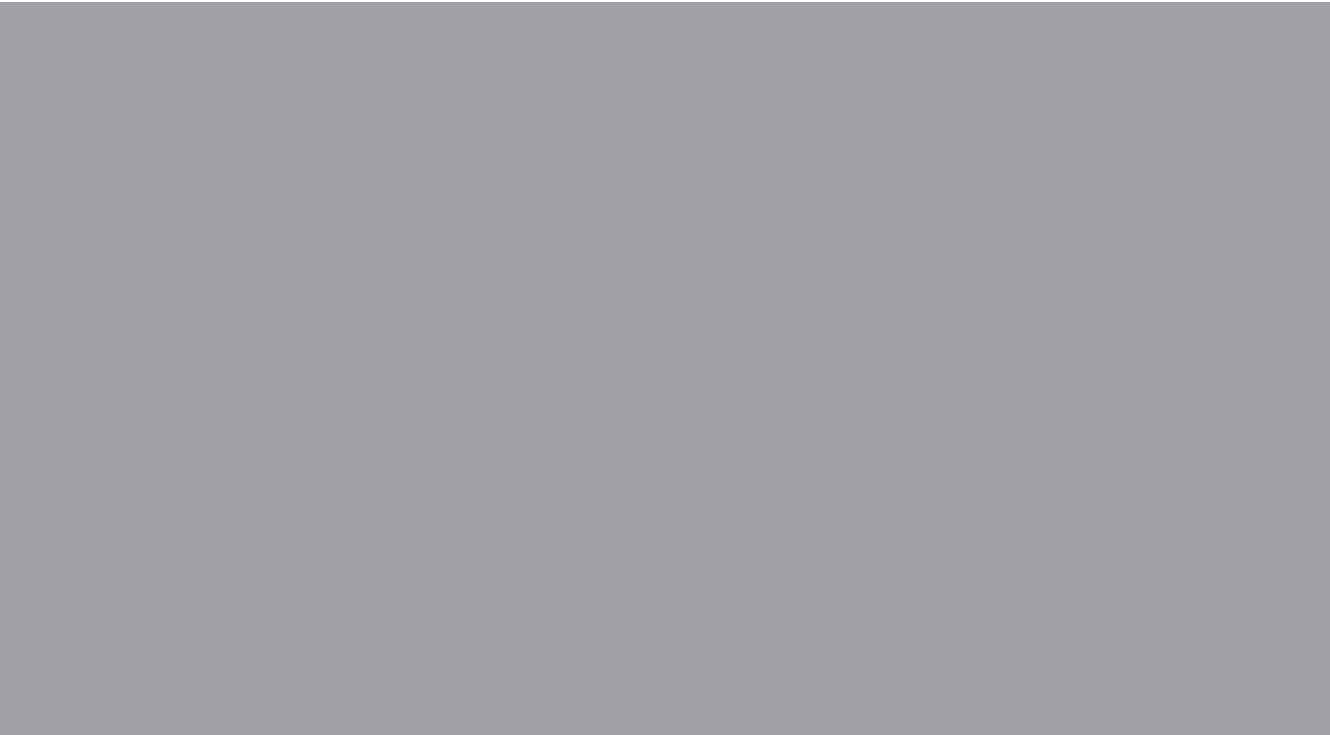
References

[1]   Human Development Report, UNDP, 2007/2008, available online at http://hdrstats.undp.org/indicators/211.html, quoted 2009-01-19.

[2]   Experience Curves for Energy Technology Policy, IEA, 2000, available online at http://iea.org/textbase/nppdf/free/2000/curve2000.pdf, quoted 2009-01-19.

[3]   Shell energy scenarios to 2050, Shell International BV, 2008, available online at http://www-static.shell.com/static/aboutshell/downloads/ our_strategy/shell_global_scenarios/SES%20booklet%2025%20of%20Jul y%202008.pdf, quoted 2009-01-19.

[4]   J. M. Kroon, N. J. Bakker, H. J. P. Smit, P. Liska, K. R. Thampi, P. Wang, S. M. Zakeeruddin, M. Grätzel, A. Hinsch, S. Hore, U. Würfel, R. Sastrawan, J. R. Durrant, E. Palomares, H. Pettersson, T. Gruszecki, J. Walter, K. Skupien, G. E. Tulloch, Prog. Photovolt: Res. Appl. 15, pp. 1-18, 2007.

[5]   K. Zweibel, Sol. Energy Mater. Sol. Cells 59(1-2), pp. 1-18, 1999.

[6]   T. Ma, X. Fang, M. Akiyama, K. Inoue, H. Noma, E. Abe, J. Electroanal. Chem. 574(1), pp. 77-83, 2004.

[7]   X. Fang, T. Ma, M. Akiyama, G. Guan, S. Tsunematsu, E. Abe, Thin Solid Films 472(1-2), pp. 242-245, 2005.

[8]   M. Toivola, F. Ahlskog, P. Lund. Sol. Energy Mater. Sol. Cells 90(17), pp. 2881-2893, 2006.

[9]   H. Lindström, E. Magnusson, A. Holmberg, S. Södergren, S. Lindquist, A. Hagfeldt, Sol. Energy Mater. Sol. Cells, 73(1) pp. 91-101, 2002.

[10]   T. Miyasaka, M. Ikegami, Y. Kijitori, J. Electrochem. Soc. 154(5), pp. A455-A461, 2007.

[11]   M. G. Kang, N.-G. Park, K. S. Ryu, S. H. Chang, K.-J. Kim., Sol. Energy Mater. Sol. Cells 90(5), pp. 574-581, 2006.

[12]   S. Ito, N.-L. C. Ha, G. Rothenberger, P. Liska, P. Comte, S.M. Zakeeruddin, P. Péchy, M.K. Nazeeruddin, M. Grätzel, ChemComm, (38), pp. 4004-4006, 2006.

[13]   J.H. Park, Y. Jun, H.-G. Yun, S.-Y. Lee, M. G. Kang, J. Electrochem. Soc. 115(7), pp. F145-F149, 2008.

[14]   Luque, S. Hegedus. Handbook of Photovoltaic Science and Engineering. Chapter 15: Dye-sensitized Solar Cells. John Wiley & Sons, 2003

[15]   A. Zaban, M. Greenshtein, J. Bisquert, ChemPhysChem 4, pp. 859-864, 2003.

[16]   A. Zaban, J. Zhang, Y. Diamant, O. Melemed, J. Bisquert, J. Phys. Chem. B 107(25), pp. 6022-6025, 2003.

[17]   B. Macht, M. Turrión, A. Barkschat, P. Salvador, K. Ellmer, H. Tributsch, Sol. Energy Mater. Sol. Cells 83(2-3), pp. 247–262, 2004.

[18]   A. Hagen, A. Barkschat, J. K. Dorhmann, H. Tributsch, Sol. Energy Mater. Sol. Cells 77(1), pp. 1-13, 2003.

[19]   P.M. Sirimanne, T. Jeranko, P. Bogdanoff, S. Fiechter, H. Tributsch, Semicond. Sci. Technol. 18(7), pp. 708–712, 2003.

[20]   F. Fabregat-Santiago, J. Bisquert, G. Garcia-Belmonte, G. Boschloo, A. Hagfeldt, Sol. Energy Mater. Sol. Cells 87(1-4), pp. 117-131, 2005.

[21]   F. Fabregat-Santiago, J. Bisquert, E. Palomares, L. Otero, D. Kuang, S. M. Zakeeruddin, M. Grätzel, J. Phys. Chem. C 111(17), pp. 6550 -6560, 2007.

[22]   R. Kern, R. Sastrawan, J. Ferber, R. Stangl, J. Luther. Electrochem. Acta 47(26), pp. 4213-4225, 2002.

[23]   J. Bisquert, G. Garcia-Belmonte, F. Fabregat-Santiago, N. S. Ferriols, P. Bogdanoff, E. Pereira, J. Phys. Chem. B 104 (10), pp. 2287-2298, 2000.

[24]   T. Hoshikawa, M. Yamada, R. Kikuchi, K. Eguchi, J. Ele. Chem. 577(2), pp. 339-348, 2005.

[25]   K. Lobato, L. M. Peter, U. Würfel, J. Phys. Chem. B, 110(33), pp.16201-16204, 2006.

[26]   S. Hore, R. Kern, Appl. Phys. Lett., 87, 263504, 2005.

[27]   P.J. Cameron, L.M. Peter, S. Hore, J. Phys. Chem. B, 109(2) pp. 930-936, 2005.

[28]   J. Xia, N. Masaki, K. Jiang, S. Yanagida, J. Phys. Chem. B, 110(50), pp. 25222-25228, 2006.

[29]   J. Xia, N. Masaki, K. Jiang, S. Yanagida, J. Phys. Chem. C, 111(22) pp. 8092-8097, 2007.

[30]   J. Xia, N. Masaki, K. Jiang, S. Yanagida, Chem. Comm., pp. 138-140, 2007.

[31]   T. Hoshikawa, M. Yamada, R. Kikuchi, K. Eguchi, J. Electrochem. Soc., 152(2), pp. E68-E73, 2005.

[32]   J. Halme, G. Boschloo, A. Hagfeldt, P. Lund, J. Phys. Chem. C, 112(14), pp. 5623-5637, 2008.

[33]   T. N. Murakami, M. Grätzel, Inorg. Chim. Acta 361(3), pp. 572-580, 2008.

[34]   Y. Saito, T. Kitamura, Y. Wada, S. Yanagida, Chem. Lett. 31(1-3), pp. 1060-1061, 2002.

[35]   A. Kay, M. Grätzel, Sol. Energy Mater. Sol. Cells 44(1), pp. 99-117, 1996.

[36]   N. Papageorgiou, P. Liska, A. Kay, M. Grätzel, J. Ele. Chem. Soc. 164(3), pp. 898-907, 1999.

[37]   M. Toivola, K. Miettunen, J. Halme, F. Ahlskog, P. Lund. Proceedings of 21st European Photovoltaic Solar Energy Conference, pp. 47-52, 2006.

[38]   A. Hauch, A. Georg, Electrochem. Acta 46(22), pp. 3457-3466, 2001.

[39]   F. O. Lenzmann, J. M. Kroon, Advances in OptoElectronics, Article ID 65073, 2007.

[40]   T. Yamaguchi, N. Tobe, D. Matsumoto, H. Arakawa. Chem. Comm. pp. 4767-4769, 2007.

[41]   H. Guangseng, J. Halme, K. Miettunen, M. Toivola, P. Lund, Proceedings of ISES World Congress 2007, pp. 1055-1058, 2007.

[42]   M. Grätzel, J. Photochem. Photobiol. A: Chem. 164(1-3), 3-14, 2004.

[43]   G. Boschloo, H. Lindström, E. Magnusson, A. Holmberg, A. Hagfeldt. J. Photochem. Photobiol. A: Chem. 148(1-3), pp. 11-15, 2002.

[44]   M. Toivola, T. Peltola, K. Miettunen, J. Halme, P. Lund, J. Nanosci. and Nanotech., in press.

[45]   R. Sastrawan, J. Beier, U. Belledin, S. Hemming, A. Hinsch, R. Kern, C. Vetter, F. M. Petrat, A. Prodi-Schwab, P. Lechner, W. Hoffmann, Sol. Energy Mater. Sol. Cells 90(11), pp. 1680–1691, 2006.

[46]   A. Kay, PhD Thesis, Ecole Polytechnique Fédérale de Lausanne, Switzerland, 1994.